AMERICAN ACADEMY OF OPHTHALMOLOGY®

Alterations in Lens Free Water Distribution Are Associated with Shape Deformation in Accommodation

Alyssa L. Lie, PhD,[1,2] *Xingzheng Pan, PhD,*[1] *Ehsan Vaghefi, PhD,*[2] *Thomas W. White, PhD,*[3] *Paul J. Donaldson, PhD*[1]

Objective: To investigate whether a redistribution of water within the crystalline lens is associated with the shape deformation that occurs during accommodation.

Design: Observational, cross sectional study.

Subjects: Eleven young adults without presbyopia (aged 18–39 years) and 9 middle-aged adults with presbyopia (aged 40–55 years).

Methods: Magnetic resonance imaging (MRI) scans of the lens were acquired on a 3 Tesla clinical MRI scanner, without and with the presentation of a 3 Diopter accommodative stimulus. The MRIs were post-processed using established methods to extract the geometric dimensions and spatial maps of water distribution of the lens.

Main Outcome Measures: Accommodative changes in the full 3-dimensional description of lens shape, the lens total-water distribution profile, and the lens free-water distribution profile.

Results: Viewing of an accommodative stimulus by young subjects elicited an elastic shape deformation of the lens consistent with accommodation that was associated with an elevated, smoother free-water distribution, primarily in the anterior region of the lens. In contrast, viewing of an accommodative stimulus by presbyopic subjects produced an atypical shape deformation of the lens that was instead associated with a lowered free-water distribution, primarily in the anterior region of the lens. No discernible changes to the lens total-water distribution were observed in response to the accommodative stimulus in either subject cohort.

Conclusions: The present study suggests that protein-mediated alterations in the free-water distribution of the anterior region of the lens influence the shape deformation in accommodation, presenting pharmacological modulation of free-water distribution as an attractive novel approach for treating presbyopia.

Financial Disclosure(s): The authors have no proprietary or commercial interest in any materials discussed in this article.

In addition to serving as a conduit of light transmission to the retina for clear vision, the crystalline lens is also the key contributor to the dynamic focusing of the young human eye. By assuming a thicker and rounder shape,[1–3] the lens increases its refractive power,[4] allowing the eye to switch its focus from distant to near images in an act called accommodation. However, the apparent shape deformation and hence refractive power change that the lens can undergo progressively declines with age,[5] and eventually results in the deterioration of near vision that manifests as presbyopia in middle age. Although there are a variety of reasonably effective ways for addressing the symptoms of presbyopia,[6] rates of uncorrected presbyopia remain high in regions where the cost of glasses and lack of access to eye care services are barriers to obtaining treatment. A recent review[7] estimated that approximately half of the 1.8 billion people globally affected by presbyopia had near visual impairment because of an unmet need for presbyopia correction, posing a significant global health and economic burden.[8]

As the scope of the problem escalates due to worldwide population aging, there is a growing impetus to develop modern solutions that can address the issues related to the availability, affordability, and accessibility of existing treatments. In this regard, pharmaceutical agents are being developed to target the underlying causes of presbyopia[6,9] with the hopes of delaying its onset or restoring the natural accommodative capacity of the aged lens. However, none of these approaches have gained sufficient traction to become established interventions. Progress on this front has largely been impeded by a lack of understanding of the physiological processes that enable the young lens to deform its shape during accommodation and how they become perturbed by middle age to produce presbyopia.

If we uphold the conventional assumption that the lens is practically incompressible because of its substantial water content, then the elastic deformation of the capsular bag observed in accommodation implies that the lens redistributes its internal contents to facilitate accommodative

https://doi.org/10.1016/j.xops.2023.100404
ISSN 2666-9145/23

shape changes. In theory, this raises a great opportunity for identifying potential molecular biomarkers within the lens substance to use as therapeutic targets for presbyopia, but this concept has not been supported by other investigations. Specifically, several studies[3,10–12] have reported that lens volume (VOL) increases with accommodation, leading to alternative proposals that the lens undergoes decompression[3,10] or fluid exchange with its surrounding humors[11,12] during accommodation. It has become apparent that we need an updated and comprehensive insight into the exact physiological mechanisms involved in lens accommodative deformation to inform the design of effective antipresbyopia treatments.

Until recently, this was impeded by the difficulty in studying the physiology of the human lens noninvasively. Thus, this study aimed to characterize the physiological changes that the lens undergoes with accommodation and compare them between young and presbyopic adults. In the lens, there are primarily 2 types of water molecules present: free-water molecules, which are not directly associated with any structural components of the lens, and bound-water molecules, which are tightly associated with the lens proteins and other structural components. We employed our previously developed multiparametric magnetic resonance imaging (MRI) protocols[13–15] to spatially map the total-water and free-water distributions within the lens, parameters that act as indicators of the physiological status of the in vivo lens. We also complement these observations with MRI-acquired geometric and volumetric measurements of the lens. Elucidating the pathophysiology behind the gradual loss of lens shape deformation central to presbyopia may lead to the identification of modifiable biomarkers that can be targeted to delay or reverse its onset.

Methods

All procedures were approved by the University of Auckland Human Participants Ethics Committee (reference: 018868) and complied with the tenets of the Declaration of Helsinki. Written informed consent was obtained from all subjects before study commencement.

Subjects

The study population was composed of 11 young (21 ± 2 years) and 9 middle-aged subjects (46 ± 2 years) with emmetropia and unaided distance visual acuities of 0.00 logarithm of the minimum angle of resolution (logMAR; Snellen 6/6) or better. All middle-aged subjects were symptomatic for presbyopia and/or had existing near-vision correction for presbyopia. Only 1 eye was selected for data collection. When both eyes satisfied the inclusion criteria, the eye with a lower refractive error was chosen.

Accommodative Capacity

Amplitude of accommodation (AoA) was measured for each subject using the minus-lens-to-blur method.[16] The subject was directed to view a 0.30 logMAR (Snellen 6/12) row of letters at a 6 m distance. Then, negative spherical lenses were placed in front of the eye and gradually increased in 0.25 diopter (D) steps until the subject reported first sustained blur. Amplitude of accommodation was recorded as the dioptric amount of minus lens required to reach this point. Objective accommodative responses to 1, 3, and 5 D accommodative stimuli were also acquired. Subjects were instructed to focus on a 0.3 logMAR (Snellen 6/12) sized 4-letter word displayed 2.1 m away while viewing through the corresponding negative lens power. This viewing distance was chosen to be consistent with that of the MRI chamber (see MRI Acquisition section). Five consecutive autorefraction measurements were obtained with an open-field autorefractor (NVision-K 5001, ShinNippon), and the objective accommodative response was determined using the average of the mean sphere values.

MRI Acquisition

All MR imaging sessions were performed at the Centre for Advanced Magnetic Resonance Imaging (CAMRI) at the University of Auckland, using a 3 Tesla clinical scanner (MAGNETOM Skyra; Siemens) and a 32-channel head receiver coil (Siemens). Before entering the scanner, all subjects completed an MRI safety form, which was evaluated by an MRI technologist or radiographer, to exclude those with contraindications for undergoing MRI. Once inside the MRI chamber, subjects were placed in a supine position on the scanner bed with their head stabilized by foam pads and were instructed to look at a screen at the rear end of the chamber (2.1 m from the subject) via a 45°-tilted mirror. The target displayed on the screen consisted of 0.3 logMAR (Snellen 6/12) sized 4-letter words that randomly changed every 5 seconds, designed to keep the reflex accommodation system engaged throughout the scan duration. The fellow eye was occluded with an eye patch to control for accommodative convergence and prevent diplopia. A falcon tube filled with room temperature water was also strapped next to their open eye (Fig 1) to serve as a reference for the total-water measurements.[13,17]

The MRI protocol comprised a localizer sequence to align the lens within the field of view, a high-resolution structural scan to acquire data for measuring lens dimensions, and a multiparametric mapping sequence to obtain spatial measurements of lens total-water and free-water concentration. The protocol was repeated twice, once in a relaxed state with no accommodative stimulus applied and another in the presence of an accommodative stimulus

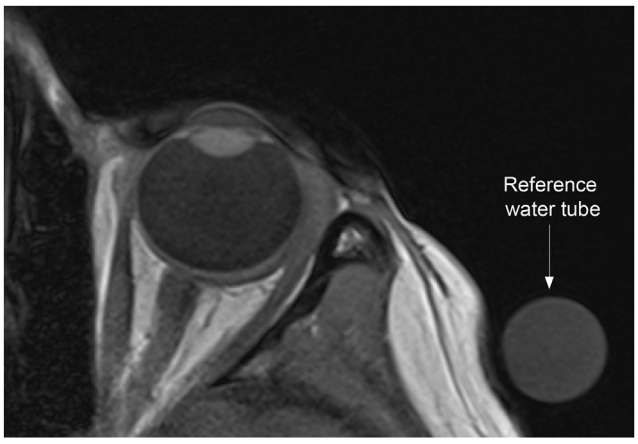

Figure 1. Postprocessing of total-water concentration of the in vivo human lens. A raw magnetic resonance imaging (MRI) scan obtained of the eye of a 45-year-old female who was representative of the presbyopic subject cohort, which includes a falcon tube of room temperature water that serves as an external water reference. This allows for the total-water concentration (ρ_{lens} value) across the in vivo lens to be calculated by normalizing the MRI proton density values measured from the lens to that of the reference water tube.

induced by a 3 D negative lens. Subjects were instructed to avoid head movement and to keep the target as clear as possible throughout image acquisition. Time was given to rest their eyes (between 30 seconds to a minute) between sequences. The scan always began in a relaxed state to minimize the potential influence of accommodative spasms on the MRI measurements. Image acquisition was typically completed within 30 minutes.

Parameters of the MRI sequences employed in this study are as described previously;[13–15] so only a brief description is provided. Lens geometry was obtained with a turbo spin-echo sequence (field of view = 179 mm^2; matrix size = 448 × 448; slice thickness = 3 mm; echo time = 116 ms; repetition time = 2000 ms; parallel imaging acceleration factor = 2; in-plane resolution = 0.4 mm^2; total imaging time = 2.5 minutes). Lens water measurements were obtained with dual proton density and T1 mapping, which utilized a volumetric interpolated breath-hold examination sequence with 2 flip angles (field of view = 159 mm^2; matrix size = 768 × 768; slice thickness = 3 mm; echo time = 2.7 ms; repetition time = 15 ms; flip angle [α] = 4° and 23°; parallel imaging acceleration factor = 2; in-plane resolution = 0.2 mm^2; total imaging time = 4.5 minutes). Proton density mapping measures the apparent concentration of H^+ protons within tissue and hence provides a measure of the total concentration of all water molecules in the lens,[18] whereas T1 mapping is dominated by the signal from mobile water molecules, hence the T1 time constant can be used as a surrogate of the concentration of free water in bodily tissues,[19] including the lens. Field inhomogeneity of the raw MR images acquired at the 2 flip angles was corrected post hoc with a B1-map (turbo-FLASH sequence, field of view = 220 mm; matrix size = 160 × 160; slice thickness = 3 mm; echo time = 2.23 ms, repetition time = 1349 ms; parallel imaging acceleration factor = 2; total imaging time = 30 seconds).

Data Extraction

For each MRI sequence, the image slice containing the thickest lens cross section visible was manually selected for data analysis. All raw MRIs were postprocessed with custom-written routines in MATLAB (MathWorks). Established methods[14,15,20] were used to extract the lens axial thickness (LT), equatorial diameter (ED), anterior (R_a) and posterior (R_p) surface radii of curvature, surface area (SA), cross sectional area (CSA), and VOL.

The postprocessing framework for proton density and T1 maps to extract lens total-water and free-water concentration and distribution, respectively, have been detailed in a previous publication.[13] Lens total-water concentration (ρ_{lens}) was expressed as a percentage unit (p.u.) of the proton density value of the external water concentration standard, whereas an estimation of the lens free-water concentration was represented by the MRI T1 time constant (ms). Distributions of total- and free-water were independently plotted for the anterior and posterior lens by fitting the ρ_{lens} or T1 values to a power function against axial distance:

$$\rho_{lens}\,(x) \;=\; \rho_{lens}(0) + b(x)^c$$

$$\mathrm{T1}\,(x) \;=\; \mathrm{T1}(0) + b(x)^c$$

where x is the distance from the lens center, b is the difference in water concentration between the lens center and surface (such that it is positive when the water content is higher at the surface), and c is the exponent that characterizes the rate of change in water concentration across the lens and therefore serves as a measure of the gradient of the water distribution. The lens was separated into anterior and posterior portions to account for not only the different geometries of these 2 regions[21,22] but also how they differentially change with age and accommodation.[23–25]

Statistical Analysis

Data are reported as mean ± standard deviation. Differences in measurements obtained from young versus presbyopic subjects were assessed with 2-tailed independent t tests. Normality of data was assessed by the Shapiro–Wilk test of normality, and homogeneity of variances was assessed by the Levene test for equality of variances. Differences in MRI measurements of the lens obtained in the relaxed state and with accommodation to a 3 D stimulus were assessed with 2-tailed paired t tests. The assumption of normality of differences was assessed by the Shapiro–Wilk test of normality. Upon the violation of this assumption, a nonparametric test (Wilcoxon sign-ranked test) was conducted instead. Significance level for all statistical tests was set at 5%. All analyses were performed in GraphPad Prism (version 9.4.1; GraphPad Software).

Results

Accommodative Characteristics in Young versus Presbyopic Subjects

Overall, the accommodative characteristics of recruited subject cohorts were in line with their expected age norms. On average, the AoA of our young cohort was 6.47 ± 2.26 D. Meanwhile, the AoA of our presbyopic cohort was 1.92 ± 0.41 D, which was significantly reduced compared with that of young subjects ($P < 0.001$; Fig 2A). These results confirmed that accommodative capacity differed between the 2 cohorts. Young subjects were also able to increase their accommodative response accordingly across the 3 accommodative stimuli, whereas presbyopic subjects could not increase their response once they had reached their maximum AoA (Fig 2B). Despite this, young subjects still demonstrated an accommodative lag that increased from 0.40 to 0.41, then to 0.69 D as the stimulus demand went from 1 to 3, and then to 5 D. Thus, we employed a 3 D stimulus to minimize fatigue and accommodative lag during the MRI scan, because this was the lowest stimulus demand at which the accommodative response between young and presbyopic subjects significantly differed ($P < 0.001$).

Accommodative Changes in the Young Lens

Table 1 contains a summary of the key lens geometric parameters extracted from MRI scans of young subjects. In response to a 3 D accommodative stimulus, young lenses underwent a 5% increase in LT, a 3% decrease in ED, a 20% steepening in R_a, and a relatively modest 6% steepening in R_p. In terms of its volumetric description, the lens exhibited a 4% reduction in SA with accommodation, but neither the CSA nor VOL showed a significant difference with accommodation. Taken together, preservation of the lens volume with accommodative deformation of the capsular bag suggests that the lens is incompressible.

Consistent with the accommodative thickening of the lens, the total-water distribution profile plotted for the accommodated lens was extended in length compared with that for the relaxed lens. However, the profiles revealed this was primarily due to the thickening of the anterior lens section, whereas the posterior lens thickness increased to a comparatively small extent (Fig 3). Irrespective of the

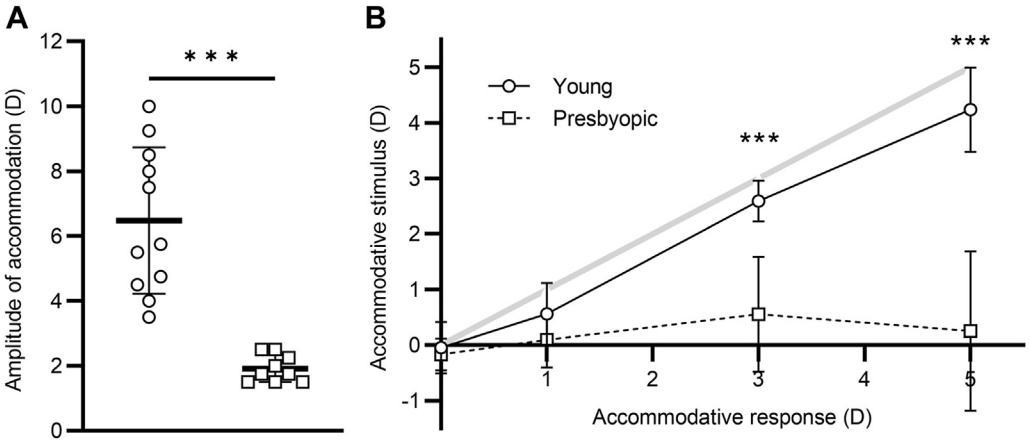

Figure 2. Young subjects have an increased accommodative capacity compared with presbyopic subjects. **(A)** Amplitude of accommodation measurements obtained from presbyopic subjects were significantly lower than those obtained from young subjects. **(B)** When the accommodative stimulus was incrementally increased from 0 to 5 diopters (D), accommodative responses increased from 0 ± 0.46 D to 4.2 ± 0.76 D in young subjects but only increased from 0 ± 0.29 D to 0.56 ± 1.44 D in presbyopic subjects. A perfectly accurate accommodative response is indicated by the solid gray line. Accommodative responses between young and presbyopic subjects did not differ at 0 and 1 D stimuli, but young subjects exhibited significantly higher accommodative responses than presbyopic subjects at 3 and 5 D stimuli. Bars are presented as mean ± standard deviation. ***$P < 0.001$; 2-tailed independent t test.

accommodative state, total-water profiles in the young lens displayed a uniform distribution pattern across both the anterior and posterior regions. Furthermore, the profiles plotted from relaxed and accommodated young lenses overlapped extensively. From this, it was inferred that accommodation had no discernible effects on total-water distribution across the young lens. Quantitative measurements of total-water concentration across the lens (Table 2) confirmed that there were no significant changes at the anterior lens surface, lens center, or posterior lens surface with accommodation. These results indicate that the observed shape deformations listed in Table 1 are unlikely to be facilitated by the entry of external fluid into the lens.

Contrary to total water, the free-water distribution profiles displayed a parabolic gradient in which free-water concentration was highest at the lens surfaces relative to the center (Fig 4). Table 2 lists the free-water concentration measurements obtained from the surfaces and center of the relaxed young lens, which further confirms this observation. This parabolic distribution of free water was present regardless of the accommodative state, with free-water concentrations remaining constant at the anterior lens surface, lens center, and posterior lens surface with accommodation to a 3 D stimulus.

With accommodation however, the free-water profile across the anterior lens section shifted to higher concentrations such that the gradient was more gradual (Fig 4), as characterized by a significantly smaller profile exponent value (Table 2). This is consistent with the hypothesis that the internal lens contents are redistributed during accommodative shape deformation. Interestingly, this redistribution was limited to only the anterior region of the lens; the exponent value of the posterior lens free-water distribution did not differ with accommodation (Fig 4 and Table 2).

Table 1. Accommodative Changes in Geometric and Volumetric MRI Measurements of Lens Shape in Young Subjects

Lens Geometric and Volumetric Parameters	Relaxed (0 D Stimulus)	Accommodated (to 3 D Stimulus)	Difference	P
LT (mm)‡	3.48 ± 0.17	3.64 ± 0.17	0.16 ± 0.10	< 0.001
ED (mm)†	9.34 ± 0.54	9.09 ± 0.43	−0.25 ± 0.24	0.007
R_a (mm)‡	11.96 ± 1.37	9.57 ± 1.70	−2.38 ± 1.29	< 0.001
R_p (mm)†	−5.15 ± 0.70	−4.85 ± 0.55	0.30 ± 0.26	0.003
SA (mm^2)*	164 ± 17	157 ± 13	−7 ± 8	0.015
CSA (mm^2)	23.60 ± 2.05	23.85 ± 1.45	0.25 ± 1.25	0.519
VOL (mm^3)	140 ± 20	137 ± 14	−3 ± 11	0.342

Difference, difference in measurement obtained from the lens in a relaxed state (zero stimulus) and an accommodated state (to a 3 D stimulus). Data are reported as mean ± standard deviation. Statistical analysis was performed using a 2-tailed paired t test.
CSA = cross sectional area; D = diopters; ED = equatorial diameter; LT = lens axial thickness; MRI = magnetic resonance imaging; R_a = anterior surface radius of curvature; R_p = posterior surface radius of curvature; SA = surface area; VOL = volume.
*$P < 0.05$.
†$P < 0.01$.
‡$P < 0.001$.

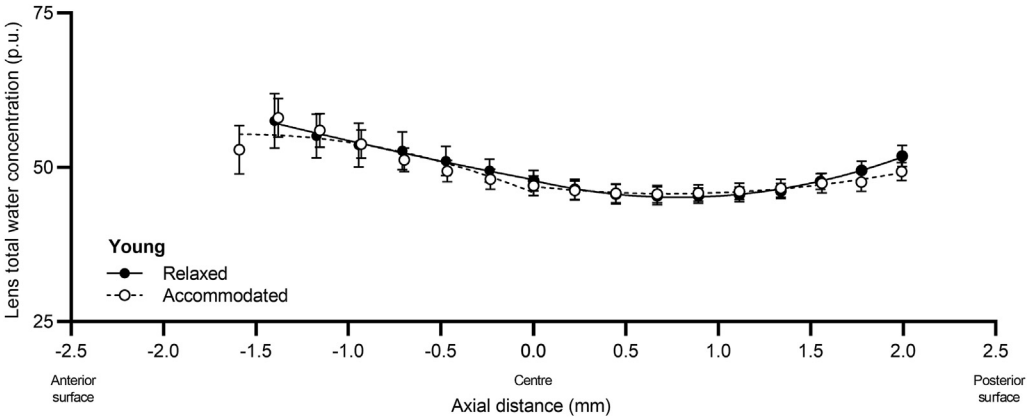

Figure 3. Lens total-water concentration and distribution in young subjects remain constant with accommodative deformation. Total-water concentration (ρ_{lens} values) extracted from magnetic resonance imaging proton density scans, plotted as a function of axial distance from the lens center, across the anterior and posterior regions of the young lens. Fittings of the ρ_{lens} values showed a relatively uniform total-water concentration gradient across the lens. Total-water distribution profiles plotted from the relaxed lens (no accommodative stimulus) and the accommodated lens (to a 3 D stimulus) overlapped extensively. Bars are presented as mean ± standard deviation.

Accommodative Changes in the Presbyopic Lens

Unlike young lenses which underwent significant shape deformation, accommodative effort to a 3 D stimulus by presbyopic subjects induced only a limited degree of lens deformation. With accommodative effort, LT increased by 4%, whereas ED, R_a, and R_p displayed no significant differences. It should follow that the volumetric parameters also show little to no change, but increases of 3%, 5%, and 6% in SA, CSA, and VOL, respectively, were observed with accommodative effort. The data, shown in Table 3, suggest that in presbyopia, shape deformation of the lens is not only inhibited but also occurs abnormally, seeing as it undergoes changes in the 3-dimensional space while remaining constant in its 2-dimensional measurements.

An inadvertent net influx of fluid upon accommodative effort could explain the unexpected increase in SA, CSA, and VOL of the presbyopic lens; however, an apparent and extensive overlap in the linear total-water distribution profiles plotted for the relaxed and accommodated states indicated there was no obvious increase in total-water concentration across the anterior or the posterior regions of the lens with accommodative effort (Fig 5). A summary description of the fitting parameters of total-water distributions in the presbyopic lens is listed in Table 4, which shows that measurements of total-water concentration extracted from the anterior lens surface, central lens, and posterior lens surface also support the above observations.

We also plotted the free-water distribution profiles of presbyopic lenses to determine whether a redistribution of internal lens contents was associated with the abnormal shape deformation described in Table 3. The free-water profiles displayed a parabolic distribution highest in concentration at the surfaces and lowest at the center that was preserved regardless of accommodative state, much like the free-water profiles plotted for young lenses (Fig 4). Contrary to young lenses, however, the accommodative effort to a 3 D stimulus by presbyopic lenses elicited a downward shift of the free-water profile in the anterior lens region that was not present in the posterior lens region

Table 2. Accommodative Changes in Lens Total-Water and Free-Water Distributions in Young Subjects

Lens Total- and Free-Water Distribution Parameters	Relaxed (0 D Stimulus)	Accommodated (to 3 D Stimulus)	Difference	P
Anterior surface ρ_{lens} (p.u.)	53.2 ± 7.5	54.6 ± 5.4	1.4 ± 8.7	0.609
Central ρ_{lens} (p.u.)	47.8 ± 5.6	47.4 ± 5.6	−0.4 ± 6.4	0.833
Posterior surface ρ_{lens} (p.u.)	55.6 ± 9.9	54.8 ± 6.4	−0.8 ± 8.9	0.776
Anterior surface T1 (ms)	1502 ± 300	1680 ± 218	178 ± 382	0.153
Anterior T1 exponent*	5.08 ± 2.38	3.12 ± 1.11	−1.96 ± 2.70	0.037
Central T1 (ms)	923 ± 114	949 ± 110	27 ± 148	0.565
Posterior surface T1 (ms)	1489 ± 277	1565 ± 281	76 ± 375	0.518
Posterior T1 exponent	8.98 ± 3.12	8.56 ± 2.83	−0.42 ± 3.48	0.697

Parameters characterizing water distribution in the young lens were extracted by fitting magnetic resonance imaging-obtained values of total-water concentration (ρ_{lens}) and free-water concentration (T1) to a power function. Exponent values for the lens total-water distribution were omitted from comparison because of the linearity of the total-water profile (shown in Fig 3). Difference, difference in measurement obtained from the lens in the relaxed state (zero stimulus) and the accommodated state (to a 3 D stimulus). Data are reported as mean ± standard deviation. Statistical analysis was performed using a 2-tailed paired *t* test.
*$P < 0.05$.

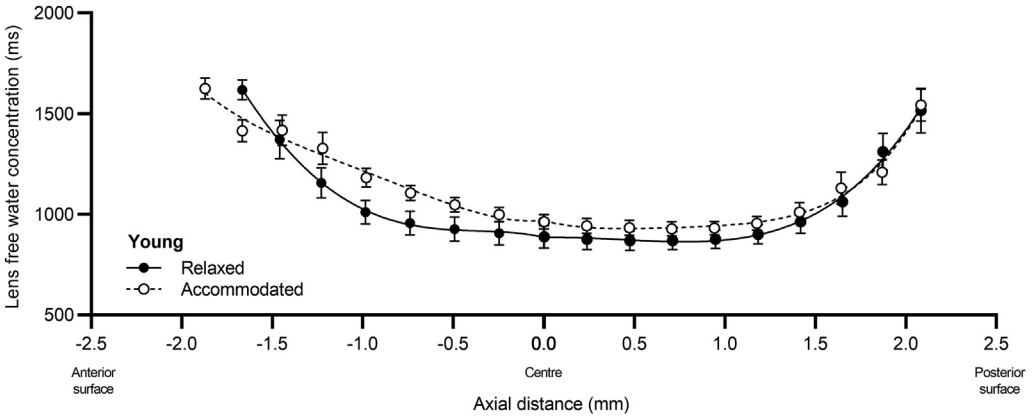

Figure 4. Lens free-water increases in concentration and becomes more smoothly distributed with accommodative deformation in young subjects. Estimates of free-water concentration (T1 values), plotted as a function of axial distance from the lens center, across the anterior and posterior regions of the young lens. Fittings of the magnetic resonance imaging T1 values showed a parabolic free-water concentration gradient across the lens that was always highest at the surface and lowest at the center. An increased concentration of free-water across the anterior region of the lens resulted in a more linear free-water distribution when the lens was accommodated to a 3 D stimulus than when it was relaxed, as indicated by a smaller profile exponent value (Table 2). The posterior lens free-water distribution was unaffected by accommodation. Bars are presented as mean ± standard deviation.

(Fig 6). The data in Table 4 showed that this displacement in anterior free-water distribution was not associated with any concurrent changes in free-water concentration at the anterior lens surface but a prominent reduction in free-water concentration at the lens center instead. Free-water concentration at the posterior surface did not differ with accommodative effort. Despite these changes, the gradient of free-water distribution remained conserved between the relaxed and accommodated states in the anterior and posterior lens regions.

Discussion

Presbyopia has been recognized for thousands of years, with mentions of the condition dating as early as the writings of Aristotle in the 4th Century BC.[26] In that time, countless studies have explored the many nuances of the accommodative system, yet there have been minimal advances in our ability to prevent or reverse the disease process. Our group has previously developed MRI protocols to study the long-term changes in the geometry[14,15] and water distribution[13] of the in vivo human lens that occur as a function of age. In this study, we have successfully adapted these established protocols for obtaining such measurements for the accommodating human lens.

It should be noted, however, that an inherent limitation of our study is the long acquisition time of MRI relative to other ocular imaging modalities used to study the accommodative process. Accommodation not only happens on a markedly fast timescale with reported reaction times in the order of seconds[27–29] but is also a dynamic process that is subject to fatigue. Continual viewing of accommodative stimuli for as little as 2 minutes has been reported to significantly increase accommodative lag.[30] Consequently, our observations may not reflect the full extent of the physiological changes of the lens with accommodation, even after having determined that all young subjects were capable of meeting the 3 D demand before undergoing

Table 3. Accommodative Changes in Geometric and Volumetric MRI Measurements of Lens Shape in Presbyopic Subjects

Lens Geometric and Volumetric Parameters	Relaxed (0 D Stimulus)	Accommodated (to 3 D Stimulus)	Difference	*P*
LT (mm)†	4.27 ± 0.21	4.46 ± 0.23	0.19 ± 0.13	0.003
ED (mm)	9.46 ± 0.53	9.49 ± 0.48	0.03 ± 0.13	0.573
R_a (mm)	9.13 ± 2.35	8.61 ± 1.55	−0.51 ± 0.99	0.160
R_p (mm)	−4.61 ± 0.50	−4.48 ± 0.48	0.14 ± 0.32	0.238
SA (mm^2)*	178 ± 12	184 ± 13	5 ± 6	0.026
CSA (mm^2)†	29.37 ± 1.24	30.96 ± 1.48	1.59 ± 0.95	0.001
VOL (mm^3)†	177 ± 12	188 ± 14	11 ± 8	0.004

Difference, difference in measurement obtained from the lens in a relaxed state (zero stimulus) and with accommodative effort (to a 3 D stimulus). Data are reported as mean ± standard deviation. Statistical analysis was performed using a 2-tailed paired *t* test.
CSA = cross sectional area; D = diopters; ED = equatorial diameter; LT = lens axial thickness; MRI = magnetic resonance imaging; R_a = anterior surface radius of curvature; R_p = posterior surface radius of curvature; SA = surface area; VOL = volume.
*$P < 0.05$.
†$P < 0.01$.

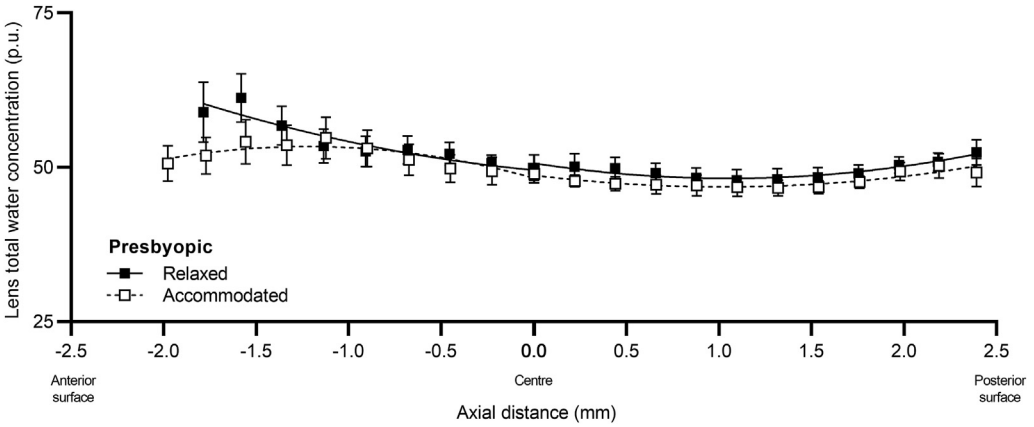

Figure 5. Lens total-water concentration and distribution in presbyopic subjects remain constant with abnormal accommodative deformation. Total-water concentration (ρ_{lens} values) extracted from magnetic resonance imaging proton density scans, plotted as a function of axial distance from the lens center, across the anterior and posterior regions of the presbyopic lens. Similar to the young lens, fittings of the ρ_{lens} values showed a relatively uniform total-water concentration gradient across the lens. Total-water distribution profiles plotted from the relaxed lens (no accommodative stimulus) with accommodative effort (to a 3 D stimulus) overlapped extensively. Bars are presented as mean ± standard deviation.

scanning. The use of higher field MRI systems can reduce scan duration and, therefore, accommodative fatigue, but, because this is not a readily available option, this limitation has to be overcome by continually finding ways to optimize the existing protocols.

An additional caveat in the present study is the inability to distinguish the subjects' accommodative capacity from their voluntary effort to accommodate. Although accommodation usually acts as a reflexive response to blur, it can be consciously controlled. Our findings therefore assume that our subjects made the best effort to focus on the target, regardless of whether their accommodative capacity allows them to do so. Based on the published values of the per Diopter change in LT however,[1,23,31,32] our MRI-measured increase of 0.16 ± 0.10 mm across the young subject cohort corresponds to an accommodative response ranging between 2.4 and 3.6 D, which closely matches the 3 D stimulus employed. Hence, we can be confident that our results are representative of the lens shape and water changes associated with the accommodative process.

In this study, we found that, although young lenses demonstrated the typical shape deformation seen in accommodation, the process did not invoke any changes to the lens volume or total-water concentration but, instead, a smoother and more elevated free-water distribution across the anterior region of the lens. Our results support the traditional notion that accommodative deformation of the young lens involves an intracapsular redistribution of the lens contents, rather than decompression[3,10] or exchange of fluid between the lens and its surrounding humors[11,12] as suggested by others.

The constancy of lens total-water concentration with accommodation implies that the observed free-water redistribution results from changes in the amount of water molecules bound to lens proteins that occur. In the lens, there are primarily 2 types of water molecules present: free-water molecules, which are free to move around within the lens or exchange with its surroundings, and bound-water molecules, which are tightly embedded within the hydration layer of proteins and other structural components in the lens. Previous

Table 4. Accommodative Changes in Lens Total-Water and Free-Water Distributions in Presbyopic Subjects

Lens Total- and Free-Water Distribution Parameters	Relaxed (0 D Stimulus)	Accommodated (to 3 D Stimulus)	Difference	*P*
Anterior surface ρ_{lens} (p.u.)	52.4 ± 5.7	51.8 ± 5.2	−0.6 ± 5.3	0.750
Central ρ_{lens} (p.u.)	48.0 ± 3.6	50.8 ± 5.2	2.8 ± 4.0	0.085
Posterior surface ρ_{lens} (p.u.)	50.7 ± 8.4	50.9 ± 5.9	0.3 ± 10.0	0.938
Anterior surface T1 (ms)	1662 ± 124	1635 ± 210	−28 ± 220	0.717
Anterior T1 exponent	5.23 ± 1.55	4.70 ± 2.02	−0.54 ± 2.54	0.570
Central T1 (ms)*	1013 ± 94	915 ± 143	−98 ± 126	0.048
Posterior surface T1 (ms)	1570 ± 231	1466 ± 179	−104 ± 232	0.215
Posterior T1 exponent	9.25 ± 2.29	9.15 ± 3.18	−0.10 ± 2.65	0.917

Parameters characterizing water distribution in the presbyopic lens were extracted by fitting magnetic resonance imaging-obtained values of total-water concentration (ρ_{lens}) and free-water concentration (T1) to a power function. Exponent values for the lens total-water distribution were omitted from the comparison because of the linearity of the total-water profile (shown in Fig 5). Difference, difference in measurement obtained from the lens in the relaxed state (zero stimulus) and with accommodative effort (to a 3 D stimulus). Data are reported as mean ± standard deviation. Statistical analysis was performed using a 2-tailed paired *t* test.
*$P < 0.05$.

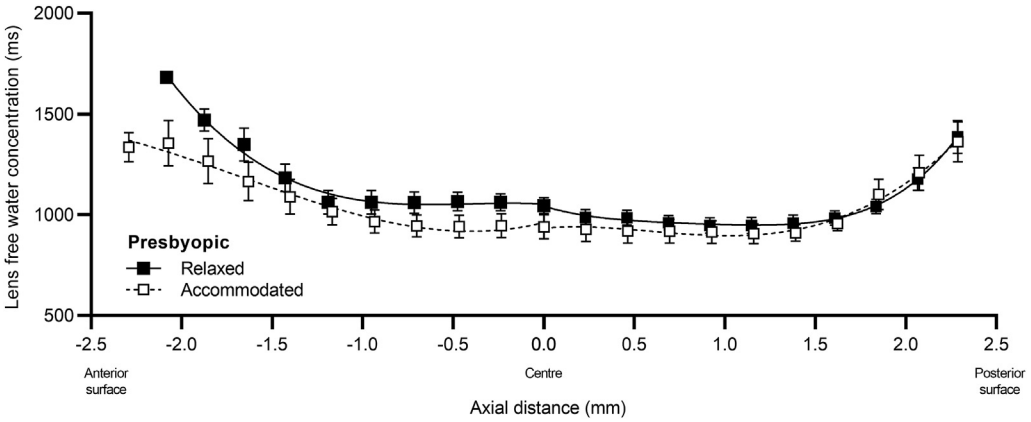

Figure 6. Lens free-water concentration decreases with abnormal accommodative deformation in presbyopic subjects. Estimates of free-water concentration (T1 values), plotted as a function of axial distance from the lens center, across the anterior and posterior regions of the young lens. Similar to the young lens, fittings of the magnetic resonance imaging T1 values showed a parabolic free-water concentration gradient across the lens that was always highest at the surface and lowest at the center. There was a decreased concentration of free water across the anterior region of the lens, particularly at the lens center (Table 4), with the accommodative effort to a 3 D stimulus than when relaxed. The posterior lens free-water distribution was unaffected by accommodative effort. Bars are presented as mean ± standard deviation.

ex vivo studies[33–36] have demonstrated that proteins in the lens respond to changes in applied external pressure by releasing their bound water in a process known as syneresis. Therefore, a possible explanation is that the alleviation of zonular tension on the lens upon accommodation signals lens proteins to undergo syneresis, effectively increasing the concentration of free water in the lens. Because bound-water influences protein behavior,[37] the reversible action of syneresis may facilitate accommodative shape deformation of the lens by altering the conformation and packing of proteins. The idea that syneresis may be involved in accommodation was initially refuted as the external pressures tested were considered too high,[38] but our findings suggest that such a mechanism is plausible even under physiologically relevant pressure changes.

The extent to which lens proteins can undergo syneresis has been reported to diminish with age, eventually becoming an irreversible process,[33] where proteins are no longer able to release their bound water in response to changes in pressure and instead can only increase their binding to free water. The biomechanical significance of this is that an impaired syneretic response alters protein conformation and packing within the lens substance in a manner that fails to deform the lens desirably, or altogether, for accommodation. Our observations that accommodative effort by the presbyopic lens produced an abnormal shape deformation concurrent with a decrease in the ratio of free to bound water in the anterior region of the lens would certainly be aligned with the above line of thinking.

The accommodative changes in free water in the lens, albeit occurring in opposite directions for young versus presbyopic subjects, were almost exclusively confined within the anterior region of the lens. We speculate this could be because anteriorly located lens proteins experience greater pressure changes from the asymmetrical localization of zonular fiber insertions,[39,40] and consequently exhibit a stronger syneretic response during accommodation. That the lens deforms nonuniformly during accommodation raises the question of whether abnormal lens deformation in presbyopia occurs as a consequence of a loss of syneretic responsiveness by the proteins in the anterior lens, a decreased ability of the zonular fibers to exert pressure changes onto the anterior lens to induce protein syneresis, or both. Variations of this subject matter have been the subject of longstanding debate, and a consensus has yet to be reached among those in the field. Nonetheless, it seems that the processes occurring within the anterior region are key for functional accommodative shape deformation of the lens.

In conclusion, the current study identified that an increase in free-water concentration across the anterior region of the lens was associated with shape deformation of the young lens during accommodation, whereas a decrease in free-water concentration across the same region was associated with an abnormal deformation of the presbyopic lens. Overall, these findings suggest that alterations in the lens free-water distribution, mediated by protein syneresis, may serve an important physiological role in the process of accommodative shape deformation, and could potentially act as a biomarker for presbyopia. This would have important diagnostic and therapeutic implications, facilitating early detection and personalized treatment strategies. Remarkably, our group has previously demonstrated that the lens free-water distribution can be subjected to modulation by pharmacologically perturbing ionic homeostasis in the lens,[41–43] hinting at the exciting prospect that we may be one step closer to an innovative therapeutic approach to combat the presbyopia epidemic.

Acknowledgments

This work was supported by NIH grant EY026911. Alyssa L. Lie gratefully acknowledges the doctoral scholarship support she received from the HOPE Selwyn Foundation and the New Zealand Association of Optometrists during the period of this research study.

Footnotes and Disclosures

Originally received: July 18, 2023.
Final revision: September 5, 2023.
Accepted: September 22, 2023.
Available online: October 3, 2023. Manuscript no. XOPS-D-23-00178R1.

[1] Department of Physiology, School of Medical Sciences, University of Auckland, Auckland, New Zealand.

[2] School of Optometry and Vision Science, University of Auckland, Auckland, New Zealand.

[3] Department of Physiology and Biophysics, School of Medicine, Stony Brook University, Stony Brook, New York.

Meeting Presentation: The material in this manuscript has been previously presented at the 8th International Conference on the Lens, Kailua-Kona, Hawaii, USA, 4−9 December, 2022; and the XXV Biennial Meeting of the International Society for Eye Research (ISER), Gold Coast, Australia, 19−23 February 2023.

Disclosure(s):

All authors have completed and submitted the ICMJE disclosures form.

The author(s) have made the following disclosure(s): A.L.L.: Travel support − Maurice and Phyllis Paykel Trust, International Society for Eye Research.

The other authors have no proprietary or commercial interest in any materials discussed in this article.

This study was supported by the National Eye Institute, National Institutes of Health, Bethesda, Maryland (Grant no.: EY026911). Author A.L.L. also received doctoral scholarship support from the HOPE Selwyn Foundation, Auckland, New Zealand, and the New Zealand Association of Optometrists, Wellington, New Zealand. The sponsor or funding organization had no role in the design or conduct of this research.

HUMAN SUBJECTS: Human subjects were included in this study. All procedures were approved by the University of Auckland Human Participants Ethics Committee (Ref: 018868) and complied with the tenets of the Declaration of Helsinki. Written informed consent was obtained from all subjects before study commencement.

No animal subjects were used in this study.

Author Contributions:

Conception and design: Lie, Pan

Data collection: Lie

Analysis and interpretation: Lie, Pan, Vaghefi, White, Donaldson

Obtained funding: White, Donaldson

Overall responsibility: Lie

Abbreviations and Acronyms:
AoA = amplitude of accommodation; **CSA** = cross sectional area; **D** = diopters; **ED** = equatorial diameter; **logMAR** = logarithm of the minimum angle of resolution; **LT** = lens axial thickness; **MRI** = magnetic resonance imaging; $\mathbf{R_a}$ = anterior lens surface radius of curvature; $\mathbf{R_p}$ = posterior lens surface radius of curvature; **SA** = surface area; **VOL** = volume.

Keywords:
Accommodation, Crystalline lens, Magnetic resonance imaging, Physiological optics, Presbyopia.

Correspondence:
Paul J. Donaldson, Department of Physiology, School of Medical Sciences, University of Auckland, Private Bag 92019, Auckland 1021, New Zealand.
E-mail: p.donaldson@auckland.ac.nz.

References

1. Dubbelman M, Van der Heijde GL, Weeber HA. Change in shape of the aging human crystalline lens with accommodation. *Vision Res*. 2005;45:117−132. https://doi.org/10.1016/j.visres.2004.07.032.
2. Khan A, Pope JM, Verkicharla PK, Suheimat M, Atchison DA. Change in human lens dimensions, lens refractive index distribution and ciliary body ring diameter with accommodation. *Biomed Opt Express*. 2018;9:1272−1282. https://doi.org/10.1364/BOE.9.001272.
3. Sheppard AL, Evans CJ, Singh KD, Wolffsohn JS, Dunne MC, Davies LN. Three-dimensional magnetic resonance imaging of the phakic crystalline lens during accommodation. *Invest Ophthalmol Vis Sci*. 2011;52:3689−3697. https://doi.org/10.1167/iovs.10-6805.
4. Lee DB. Error tolerance in Helmholtzian accommodation. *Ophthalmology*. 2002;109:1589−1590. https://doi.org/10.1016/s0161-6420(02)01196-x.
5. Duane A. An attempt to determine the normal range of accommodation at various ages, being a revision of Donder's experiments. *Trans Am Ophthalmol Soc*. 1908;11:634−641.
6. Katz JA, Karpecki PM, Dorca A, et al. Presbyopia − a review of current treatment options and emerging therapies. *Clin Ophthalmol*. 2021;15:2167−2178. https://doi.org/10.2147/OPTH.S259011.
7. Fricke TR, Tahhan N, Resnikoff S, et al. Global prevalence of presbyopia and vision impairment from uncorrected presbyopia: systematic review, meta-analysis, and modelling. *Ophthalmology*. 2018;125:1492−1499. https://doi.org/10.1016/j.ophtha.2018.04.013.
8. Berdahl J, Bala C, Dhariwal M, Lemp-Hull J, Thakker D, Jawla S. Patient and economic burden of presbyopia: A systematic literature review. *Clin Ophthalmol*. 2020;14:3439−3450. https://doi.org/10.2147/OPTH.S269597.
9. Charman WN. Non-surgical treatment options for presbyopia. *Expert Rev Ophthalmol*. 2018;13:219−231. https://doi.org/10.1080/17469899.2018.1506330.
10. Strenk SA, Strenk LM, Semmlow JL, DeMarco JK. Magnetic resonance imaging study of the effects of age and accommodation on the human lens cross-sectional area. *Invest Ophthalmol Vis Sci*. 2004;45:539−545. https://doi.org/10.1167/iovs.03-0092.
11. Gerometta R, Zamudio AC, Escobar DP, Candia OA. Volume change of the ocular lens during accommodation. *Am J Physiol Cell Physiol*. 2007;293:C797−C804. https://doi.org/10.1152/ajpcell.00094.2007.
12. Zamudio AC, Candia OA, Kong CW, Wu B, Gerometta R. Surface change of the mammalian lens during accommodation. *Am J Physiol Cell Physiol*. 2008;294:C1430−C1435. https://doi.org/10.1152/ajpcell.90623.2007.
13. Lie AL, Pan X, White TW, Vaghefi E, Donaldson PJ. Age-dependent changes in total and free water content of in vivo human lenses measured by magnetic resonance imaging. *Invest Ophthalmol Vis Sci*. 2021;62:33−33. https://doi.org/10.1167/iovs.62.9.33.

14. Pan X, Lie AL, White TW, Donaldson PJ, Vaghefi E. Development of an in vivo magnetic resonance imaging and computer modelling platform to investigate the physiological optics of the crystalline lens. *Biomed Opt Express*. 2019;10:4462–4478. https://doi.org/10.1364/BOE.10.004462.
15. Lie AL, Pan X, White TW, Donaldson PJ, Vaghefi E. Using the lens paradox to optimize an in vivo MRI-based optical model of the aging human crystalline lens. *Transl Vis Sci Technol*. 2020;9:39–39. https://doi.org/10.1167/tvst.9.8.39.
16. Rosenfield M, Logan N, Edwards KH, eds. *Optometry: Science, Techniques and Clinical Management*. Butterworth-Heinemann Elsevier; 2009.
17. Babizhayev MA, Nikolayev GN, Goryachev SN, Bours J. NMR spin-echo studies of hydration properties of the molecular chaperone alpha-crystallin in the bovine lens. *Biochim Biophys Acta*. 2002;1598:46–54. https://doi.org/10.1016/s0167-4838(02)00314-x.
18. Tofts PS. Proton density of tissue water. In: Tofts P, ed. *Quantitative MRI of the Brain: Measuring Changes Caused by Disease*. 1st ed. Wiley; 2003:85–108.
19. Fullerton GD, Potter JL, Dornbluth NC. NMR relaxation of protons in tissues and other macromolecular water solutions. *Magn Reson Imaging*. 1982;1:209–226. https://doi.org/10.1016/0730-725X(82)90172-2.
20. Pan X, Muir ER, Sellitto C, et al. Age-dependent changes in the water content and optical power of the in vivo mouse lens revealed by multi-parametric MRI and optical modeling. *Invest Ophthalmol Vis Sci*. 2023;64:24–24. https://doi.org/10.1167/iovs.64.4.24.
21. Atchison DA, Markwell EL, Kasthurirangan S, Pope JM, Smith G, Swann PG. Age-related changes in optical and biometric characteristics of emmetropic eyes. *J Vis*. 2008;8:29, 1–20. https://doi.org/10.1167/8.4.29.
22. Maceo Heilman B. *Evaluation of the Crystalline Lens Gradient Refractive Index Using Laser Ray Tracing and Optical Coherence Tomography*. University of Miami; 2015.
23. Jones CE, Atchison DA, Pope JM. Changes in lens dimensions and refractive index with age and accommodation. *Optom Vis Sci*. 2007;84:990–995. https://doi.org/10.1097/OPX.0b013e318157c6b5.
24. Kasthurirangan S, Markwell EL, Atchison DA, Pope JM. In vivo study of changes in refractive index distribution in the human crystalline lens with age and accommodation. *Invest Ophthalmol Vis Sci*. 2008;49:2531–2540. https://doi.org/10.1167/iovs.07-1443.
25. Kasthurirangan S, Markwell EL, Atchison DA, Pope JM. MRI study of the changes in crystalline lens shape with accommodation and aging in humans. *J Vis*. 2011;11. https://doi.org/10.1167/11.3.19.
26. Wade NJ. *A Natural History of Vision*. MIT Press; 2000.
27. Lockhart TE, Shi W. Effects of age on dynamic accommodation. *Ergonomics*. 2010;53:892–903. https://doi.org/10.1080/00140139.2010.489968.
28. Heron G, Charman WN, Gray LS. Accommodation dynamics as a function of age. *Ophthalmic Physiol Opt*. 2002;22:389–396. https://doi.org/10.1046/j.1475-1313.2002.00070.x.
29. Mordi JA, Ciuffreda KJ. Dynamic aspects of accommodation: age and presbyopia. *Vision Res*. 2004;44:591–601. https://doi.org/10.1016/j.visres.2003.07.014.
30. Tosha C, Borsting E, Ridder III WH, Chase C. Accommodation response and visual discomfort. *Ophthalmic Physiol Opt*. 2009;29:625–633. https://doi.org/10.1111/j.1475-1313.2009.00687.x.
31. Ostrin L, Kasthurirangan S, Win-Hall D, Glasser A. Simultaneous measurements of refraction and A-scan biometry during accommodation in humans. *Optom Vis Sci*. 2006;83:657–665. https://doi.org/10.1097/01.opx.0000232810.61191.02.
32. Richdale K, Sinnott LT, Bullimore MA, et al. Quantification of age-related and per diopter accommodative changes of the lens and ciliary muscle in the emmetropic human eye. *Invest Ophthalmol Vis Sci*. 2013;54:1095–1105. https://doi.org/10.1167/iovs.12-10619.
33. Bettelheim FA, Lizak MJ, Zigler Jr JS. Syneretic response of aging normal human lens to pressure. *Invest Ophthalmol Vis Sci*. 2003;44:258–263. https://doi.org/10.1167/iovs.02-0422.
34. Bettelheim FA, Lizak MJ, Zigler Jr JS. Relaxographic studies of aging normal human lenses. *Exp Eye Res*. 2002;75:695–702. https://doi.org/10.1006/exer.2002.2056.
35. Bettelheim FA. Syneretic response to pressure in ocular lens. *J Theor Biol*. 1999;197:277–280. https://doi.org/10.1006/jtbi.1998.0855.
36. Lizak MJ, Zigler Jr JS, Bettelheim FA. Syneretic response to incremental pressures in calf lenses. *Curr Eye Res*. 2005;30:21–25. https://doi.org/10.1080/02713680490894216.
37. Bellissent-Funel MC, Hassanali A, Havenith M, et al. Water determines the structure and dynamics of proteins. *Chem Rev*. 2016;116:7673–7697. https://doi.org/10.1021/acs.chemrev.5b00664.
38. Schachar RA. Accommodation, presbyopia, and the lenticular Syneretic response. *Curr Eye Res*. 2005;30:927. https://doi.org/10.1080/02713680500246965.
39. Bassnett S. Zinn's zonule. *Prog Retin Eye Res*. 2021;82:100902. https://doi.org/10.1016/j.preteyeres.2020.100902.
40. Ludwig K, Wegscheider E, Hoops JP, Kampik A. In vivo imaging of the human zonular apparatus with high-resolution ultrasound biomicroscopy. *Graefes Arch Clin Exp Ophthalmol*. 1999;237:361–371. https://doi.org/10.1007/s004170050245.
41. Vaghefi E, Kim A, Donaldson PJ. Active maintenance of the gradient of refractive index is required to sustain the optical properties of the lens. *Invest Ophthalmol Vis Sci*. 2015;56:7195–7208. https://doi.org/10.1167/iovs.15-17861.
42. Chen Y, Gao J, Li L, et al. The ciliary muscle and zonules of Zinn modulate lens intracellular hydrostatic pressure through transient receptor potential vanilloid channels. *Invest Ophthalmol Vis Sci*. 2019;60:4416–4424. https://doi.org/10.1167/iovs.19-27794.
43. Chen Y, Petrova RS, Qiu C, Donaldson PJ. Intracellular hydrostatic pressure regulation in the bovine lens: a role in the regulation of lens optics? *Am J Physiol Regul Integr Comp Physiol*. 2022;322:R263–R279. https://doi.org/10.1152/ajpregu.00309.2021.